Multi-Static Passive SAR Imaging Based on Bayesian Compressive Sensing

Qisong Wu[†], Yimin D. Zhang[†], Moeness G. Amin[†], and Braham Himed[‡]

[†] Center for Advanced Communications, Villanova University, Villanova, PA 19085, USA
[‡] RF Technology Branch, Air Force Research Lab (AFRL/RYMD), WPAFB, OH 45433, USA

ABSTRACT

Passive radar systems, which utilize broadcast and navigation signals as sources of opportunity, have attracted significant interests in recent years due to their low cost, covertness, and the availability of different illuminator sources. In this paper, we propose a novel method for synthetic aperture imaging in multi-static passive radar systems based on a group sparse Bayesian learning technique. In particular, the problem of imaging sparse targets is formulated as a group sparse signal reconstruction problem, which is solved using a complex multi-task Bayesian compressive sensing (CMT-BCS) method to achieve a high resolution. The proposed approach significantly improves the imaging resolution beyond the range resolution. Compared to the other group sparse signal reconstruction methods, such as the block orthogonal matching pursuit (BOMP) and group Lasso, the CMT-BCS provides significant performance improvement for the reconstruction of sparse targets in the redundant dictionary with high coherence. Simulations results demonstrate the superior performance of the proposed approach.

Keywords: Multi-static passive radar, synthetic aperture radar, compressive sensing, sparse Bayesian learning, high-resolution imaging

1. INTRODUCTION

Synthetic aperture radar (SAR) is a powerful sensing technique that provides high-resolution images of the scene of interest.[1] While SAR has been traditionally studied for active radar systems, its application to passive radar platforms has attracted increasing interests in recent years. Passive radar systems utilize broadcast, navigation, and communication signals as sources of opportunity to achieve low-cost and covert operation by exploiting the availability of rich illuminator sources.[2,3]

Passive radars are different from active radar systems in a number of aspects, including the extremely narrow signal bandwidth, multi-static operation, low operating frequency, and low signal-to-noise ratio (SNR).[4] In particular, the extremely narrow signal bandwidth used in passive radar systems, which typically range from hundreds of kilohertz to a few megahertz, results in poor SAR image resolutions.[1] For example, Digital Video Broadcasting-Terrestrial (DVB-T) channels use a 7.8 MHz bandwidth which yields a bistatic range resolution of approximately 20 m. The Digital Audio Broadcast (DAB) and digital cellular systems use much lower frequency bandwidths and thus yield poorer range resolutions. When conventional Fourier transform based techniques, such as the well-known backprojection technique[5] and its many variations, are used for SAR imaging, the resulting image quality may not be satisfactory in many sensing applications.

In this paper, we take advantage of the availability of multiple illuminators in a multi-static passive radar system to achieve improved SAR imaging capability. The signals emitted from multiple, spatially distributed, illuminators, when properly exploited, offer significant spatial and frequency diversity for this purpose. However, because the observations associated with different illuminators are sparse and generally disconnected, the direct application of Fourier transform based techniques would cause undesirable high sidelobes and artifacts. In addition, these methods have difficulties to achieve coherent fusion of the signals corresponding to different illuminators because the scattering coefficients of the targets are likely to differ for each bistatic pair.[6]

Further author information: Qisong Wu and Yimin D. Zhang (e-mails: {qisong.wu,yimin.zhang}@villanova.edu).

When sparse scenes are concerned, super-resolution techniques can be applied to achieve improved image resolution. In the underlying multi-static SAR imaging problem, the sparse scatterers can be considered group sparse with respect to the available illuminators in the sense that the sparse scene shares the same support of scatterer positions, whereas the scattering coefficients are different for each bistatic pair. As such, we can make use of the group sparsity model for significant performance enhancement of sparse signal recovery.[7,8] A large number of algorithms, such as group Lasso (gLasso)[7] and block OMP (BOMP),[8] have been developed for group sparse signal recovery. A major issue encountered in these group sparse recovery techniques, however, is that reliable recovery is guaranteed only when the so-called group restricted isometry property (G-RIP) is satisfied,[9] i.e., the columns extracted from the measurement matrix are approximately orthogonal. As the image resolution becomes finer, the coherence between the dictionary entries increases, thereby degrading the reconstruction reliability and performance of these algorithms.[10]

Sparse Bayesian learning algorithms, on the other hand, form a different class of effective tools for sparse signal reconstruction.[11–14] It has been demonstrated that sparse Bayesian learning algorithms have a higher reconstruction reliability when the dictionary entries have a high coherence.[12] Bayesian compressive sensing (BCS)[11] has been successfully applied in microwave imaging, direction finding, space-time adaptive processing and time-frequency analysis.[15–18] The multi-task CS (mt-CS) algorithm extends the BCS to solve group sparse problems by exploiting multiple measurement vectors that share the same sparse support.[14] It is noted that both algorithms were originally designed to recover real-valued sparse solutions as encountered in, for example, image and video processing. Furthermore, a complex multi-task Bayesian CS (CMT-BCS) algorithm has been developed to deal with complex values.[19] Compared to those which directly expand a complex entry into independent real and imaginary components, the CMT-BCS achieves improved performance by acknowledging the fact that the real and imaginary parts are merely the projection of the same complex value and thus should share the same group sparsity. The CMT-BCS algorithm is used in the underlying problem because SAR imaging problems involve complex values in the received signals, reflectivity coefficients, as well as the sensing matrices.

In this paper we focus on the basic problem of acquiring high-resolution images based upon extremely narrowband signals using multi-static observations. We first derive a forward model in a multi-static passive SAR system, and then convert the sparse target imaging into a group sparse signal reconstruction problem. The CMT-BCS approach is applied to such a problem to achieve super-resolution sparse target imaging. Simulation results verify that the processed results using the CMT-BCS outperform those obtained from backprojection as well as BOMP and gLasso algorithms.

The remainder of the paper is organized as follows. Section 2 introduces a forward model in the multi-static passive imaging system. Section 3 briefly describes the CMT-BCS approach for effective reconstruction of complex sparse signals. Section 4 presents simulation results for multi-static passive SAR imaging. Finally, Section 5 concludes this paper.

Notations: We use lower-case (upper-case) bold characters to represent vectors (matrices). In particular, $\mathbf{I}_N$ denotes the $N \times N$ identity matrix. $\overline{(.)}$ denotes complex conjugation, whereas $(.)^T$ and $(.)^H$, respectively, denote the transpose and conjugate transpose of a matrix or vector. $\mathrm{diag}(\mathbf{x})$ represents a diagonal matrix that uses the elements of $\mathbf{x}$ as its diagonal elements. $\|\cdot\|$ implies the Euclidean (l_2) norm of a vector, whereas $\|\cdot\|_1$ denotes the l_1 norm. $\mathrm{Tr}(.)$ denotes the trace of a matrix. $\mathrm{P_r}(\cdot)$ expresses the probability density function (pdf), and $\mathcal{N}(x|a,b)$ denotes the random variable x follows a Gaussian distribution with mean a and variance b. In addition, $\mathrm{Re}(x)$ and $\mathrm{Im}(x)$ are the real and imaginary parts of complex element x, respectively.

2. FORWARD MODEL

Consider a multi-static passive SAR system consisting of L stationary transmitters and a moving receiver, as depicted in Fig. 1. The receiver, which is mounted on an airborne platform, has the capability of receiving reflected signals from the targets and direct-path signals from the transmitters.

Denote the position of the lth stationary transmitter as $\mathbf{t}^{(l)}$ with $l = 1 \cdots L$, and the n-th azimuth location of the moving receiver as $\mathbf{s}_n$, $n = 1, \cdots, N$. The received signal corresponding to the lth transmitter is expressed

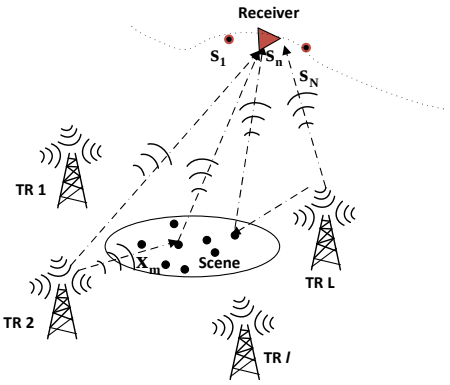

Figure 1. Geometry of a multi-static passive SAR system.

by,[20]

$$f(t,\mathbf{s}_n,\mathbf{t}^{(l)}) \approx \int \exp\left(-j\omega\left[t-\frac{R(\mathbf{s}_n,\mathbf{x},\mathbf{t}^{(l)})}{c}\right]\right)\cdot\omega^2\hat{p}(\omega)\rho(\mathbf{x},\mathbf{s}_n,\mathbf{t}^{(l)})A(\omega,\mathbf{x},\mathbf{s}_n,\mathbf{t}^{(l)})d\omega d\mathbf{x}, \tag{1}$$

where t denotes time, c is the speed of light, $R(\mathbf{s}_n,\mathbf{x},\mathbf{t}^{(l)}) = \|\mathbf{x}-\mathbf{s}_n\| + \|\mathbf{x}-\mathbf{t}^{(l)}\|$ is the bistatic range, and $\rho(\mathbf{x},\mathbf{s}_n,\mathbf{t}^{(l)})$ is the scattering amplitude of the target corresponding to the lth transmitter at position $\mathbf{x}$ when the receiver is positioned at $\mathbf{s}_n$. In addition, $\hat{p}(\omega)$ is the Fourier transform of the transmitted waveform $p(t)$, ω is the transmitted frequency, and $A(\omega,\mathbf{x},\mathbf{s}_n,\mathbf{t}^{(l)})$ is given by

$$A(\omega,\mathbf{x},\mathbf{s}_n,\mathbf{t}^{(l)}) = \frac{J_R(\omega,\mathbf{x},\mathbf{s}_n)\cdot J_T(\omega,\mathbf{x},\mathbf{t}^{(l)})}{(2\pi)^2\|\mathbf{x}-\mathbf{s}_n\|\cdot\|\mathbf{x}-\mathbf{t}^{(l)}\|}, \tag{2}$$

where $J_T(\omega,\mathbf{x},\mathbf{t}^{(l)})$ and $J_R(\omega,\mathbf{x},\mathbf{s}_n)$ are the transmit and receive antenna gains toward the target, respectively. For narrowband waveforms, the carrier frequency of ω_0 is used to replace ω in Eq. (1), and the received signal (1) can be rewritten as,[21,22]

$$f(t,\mathbf{s}_n,\mathbf{t}^{(l)}) \approx \int \exp\left[-j\omega_0\left(t-\frac{R(\mathbf{s}_n,\mathbf{x},\mathbf{t}^{(l)})}{c}\right)\right]\cdot\tilde{p}\left(t-\frac{R(\mathbf{s}_n,\mathbf{x},\mathbf{t}^{(l)})}{c}\right)\rho(\mathbf{x},\mathbf{s}_n,\mathbf{t}^{(l)})A(\omega_0,\mathbf{x},\mathbf{s}_n,\mathbf{t}^{(l)})d\mathbf{x}, \tag{3}$$

where $\tilde{p}(t)$ is the slowly time-varying complex envelope of $p(t)$. The direct-path (reference) waveform is expressed as

$$f_{\text{ref}}(t,\mathbf{s}_n,\mathbf{t}^{(l)}) \approx \exp\left(-j\omega_0\left[t-\frac{\|\mathbf{s}_n-\mathbf{t}^{(l)}\|}{c}\right]\right)\tilde{p}\left(t-\frac{\|\mathbf{s}_n-\mathbf{t}^{(l)}\|}{c}\right)\cdot\frac{J_R(\omega_0,\mathbf{s}_n)\cdot J_T(\omega_0,\mathbf{t}^{(l)})}{(2\pi)^2\|\mathbf{s}_n-\mathbf{t}^{(l)}\|}, \tag{4}$$

where $J_T(\omega_0,\mathbf{t}^{(l)})$ and $J_R(\omega_0,\mathbf{s}_n)$ are the transmit and receive antenna gains. We use the reference waveform $f_{\text{ref}}(t,\mathbf{s}_n,\mathbf{t}^{(l)})$ to perform matched filtering of $f(t,\mathbf{s}_n,\mathbf{t}^{(l)})$, resulting in

$$y(\tau,\mathbf{s}_n,\mathbf{t}^{(l)}) = \int f(t,\mathbf{s}_n,\mathbf{t}^{(l)})\overline{f_{\text{ref}}(t-\tau,\mathbf{s}_n,\mathbf{t}^{(l)})}dt = \int C_0\theta_n(\tau,\mathbf{x},\mathbf{s}_n,\mathbf{t}^{(l)})w_n(\mathbf{x})d\mathbf{x}, \tag{5}$$

where τ is the sampling delay that corresponds to the range,

$$C_0(\mathbf{s}_n,\mathbf{t}^{(l)}) = \frac{\overline{J_R(\omega_0,\mathbf{s}_n)}\cdot\overline{J_T(\omega_0,\mathbf{t}^{(l)})}}{(2\pi)^2\|\mathbf{s}_n-\mathbf{t}^{(l)}\|} \tag{6}$$

is a scalar, which is independent of the scene, and

$$\theta_n(\tau,\mathbf{x},\mathbf{s}_n,\mathbf{t}^{(l)}) = \chi(\tau,\mathbf{s}_n,\mathbf{t}^{(l)})\exp(-j\omega_0\eta_n(\mathbf{x},\mathbf{s}_n,\mathbf{t}^{(l)})), \tag{7}$$

is the observation kernel corresponding to the lth transmitter at position $\mathbf{s}_n$. In addition,

$$\chi(\tau, \mathbf{s}_n, \mathbf{t}^{(l)}) = \int \tilde{p}\left(t - \frac{R(\mathbf{s}_n, \mathbf{x}, \mathbf{t}^{(l)})}{c}\right) \overline{\tilde{p}\left(t - \tau - \frac{\|\mathbf{s}_n - \mathbf{t}^{(l)}\|}{c}\right)} dt \tag{8}$$

is the autocorrelation function of the transmitted waveform $\tilde{p}(t)$ that determines the range resolution of the radar system, $\eta_n(\mathbf{x}, \mathbf{s}_n, \mathbf{t}^{(l)}) = [R(\mathbf{s}_n, \mathbf{x}, \mathbf{t}^{(l)}) - \|\mathbf{s}_n - \mathbf{t}^{(l)}\|]/c$ denotes the difference of time delay, and

$$w_n(\mathbf{x}, \mathbf{t}^{(l)}) = \rho(\mathbf{x}, \mathbf{s}_n, \mathbf{t}^{(l)}) A(\omega_0, \mathbf{x}, \mathbf{s}_n, \mathbf{t}^{(l)}), \tag{9}$$

denotes the complex scattering coefficient. It should be noted that the scattering coefficients are dependent on the transmitter position $\mathbf{t}^{(l)}$ and the receiver position $\mathbf{s}_n$. In the conventional monostatic SAR imaging system, it is reasonable to assume that the scattering coefficient of each scatterer is invariant provided that the synthetic aperture is small. The scattering coefficients from diverse illuminating aspects, however, are generally distinct when a number of widely distributed transmitters is exploited. As such, the scattering coefficients are assumed to be invariant in each bistatic pair, and thus are independent of the receiver position as given by $w_n(\mathbf{x}, \mathbf{t}^{(l)})$ in Eq. (9), whereas they vary across bistatic pairs. As a result, there are L groups of incoherent echo data of the scene due to the L bistatic pairs.

Let us discretize the sparse target scene into M pixels. The sparse scene is represented by Q strong point targets in the entire M-pixel region, where $Q \ll M$, whereas the reflectivity of the other $M-Q$ pixels is assumed to be negligible. Such a scene is regarded as Q-sparse. In this case, (5) becomes

$$y(\tau, \mathbf{s}_n, \mathbf{t}^{(l)}) = \sum_{m=1}^{M} C_0(\mathbf{s}_n, \mathbf{t}^{(l)}) \theta_{mn}(\tau, , \mathbf{t}^{(l)}) w_{mn}. \tag{10}$$

Denote $y(\tau, \mathbf{s}_n, \mathbf{t}^{(l)})/C_0(\mathbf{s}_n, \mathbf{t}^{(l)})$ by $y_n(\tau, \mathbf{t}^{(l)})$ for simplicity. Then, by stacking the observations over all sampled delays, i.e., $\mathbf{y}_n^{(l)} = [y_n(\tau_1, \mathbf{t}^{(l)}), ..., y_n(\tau_B, \mathbf{t}^{(l)})]^T$, where B is the number of range cells being observed, we obtain

$$\mathbf{y}_n^{(l)} = \mathbf{\Theta}_n^{(l)} \mathbf{w}_n^{(l)} + \boldsymbol{\epsilon}_n^{(l)}, \tag{11}$$

where $\mathbf{\Theta}_n^{(l)} = [\boldsymbol{\theta}_n^T(\tau_1, \mathbf{t}^{(l)}), \cdots, \boldsymbol{\theta}_{Mn}^T(\tau_B, \mathbf{t}^{(l)})]^T$, in which $\boldsymbol{\theta}_n(\tau, \mathbf{t}^{(l)}) = [\theta_{1n}(\tau, \mathbf{t}^{(l)}), \cdots, \theta_{Mn}(\tau, \mathbf{t}^{(l)})]$, is the observation matrix corresponding to azimuth position $\mathbf{s}_n$ corresponding to all M pixels of $w_{mn}^{(l)}$ collected in $\mathbf{w}_n^{(l)} = [w_{1n}^{(l)}, ..., w_{Mn}^{(l)}]^T$ in the lth bistatic pair, and $\boldsymbol{\epsilon}_n^{(l)}$ is a vector that accounts for the additive measurement noise.

By stacking those echoes with respect to the observation aperture positions $\mathbf{s}_n$ in the lth bistatic pair, we have

$$\mathbf{y}^{(l)} = \mathbf{\Phi}^{(l)} \mathbf{w}^{(l)} + \boldsymbol{\epsilon}^{(l)}, \quad l \in [1, \cdots, L], \tag{12}$$

where $\mathbf{y}^{(l)} = \left[\mathbf{y}_1^{(l)^T}, \cdots, \mathbf{y}_N^{(l)^T}\right]^T$, $\mathbf{\Phi}^{(l)} = \left[\mathbf{\Theta}_1^{(l)^T}, \cdots, \mathbf{\Theta}_N^{(l)^T}\right]^T$, and $\boldsymbol{\epsilon} = \left[\boldsymbol{\epsilon}_1^{(l)^T}, \cdots, \boldsymbol{\epsilon}_N^{(l)^T}\right]^T$. It should be noted that the supports of the sparse targets are approximately identical across the L groups (i.e., the non-zero entries of $\mathbf{w}^{(l)}$ lie in the same positions across different values of l), whereas their scattering coefficients are different.

Expression (12) is a typical discrete forward model of group sparse scenes for a passive imaging radar system. As such, the radar imaging problem in the underlying multi-static passive SAR system can be regarded as the reconstruction of L-group sparse scattering coefficients.

3. COMPLEX MULTI-TASK BAYESIAN COMPRESSIVE SENSING

Conventional group inversion algorithms, such as BOMP and gLasso, guarantee reliable estimations only when the dictionary meets the so-called G-RIP condition.[9] Unfortunately, such a condition cannot be easily verified since it is computationally demanding.[23] Indeed, the G-RIP condition requires that the dictionary behaves like

an isometry system on sparse signal. In a high-resolution passive radar imaging system, however, the coherence of the dictionary $\mathbf{\Phi}$ may become very high. The literature has suggested that sparse Bayesian learning algorithms based on relevance vector machine (RVM) generally yield improved performance in such situations.[12]

The BCS and its extended mt-CS were originally designed to handle real-valued reconstruction problems, such as those encountered in image and video processing.[11,14] To process complex data, a simple approach consists of decomposing a complex value into its real and imaginary components and treat them independently.[15,16,24] Such treatments, however, ignore the fact that both real and imaginary components are merely the projection of the same complex number and, as such, they share the group sparsity between them. For example, both real and imaginary components should assume zero reflectivity coefficients when considering non-reflective positions in the scene. Treating the real and imaginary components independently unnecessarily expands the dimension of sparsity entries and thus degrades the reconstruction performance. Towards this end, a novel CMT-BCS is introduced to reconstruct sparse signals in L groups with identical or highly correlated support.[19]

We start with a prior distribution of the target reflectivities, in which the real and imaginary components follow an independent Gaussian distribution with mean zero and pixel-dependent variance α_m , i.e.,

$$\mathbf{w}_m^{(l)} \sim \mathcal{N}(\mathbf{w}_m^{(l)}|\mathbf{0}, \alpha_m \mathbf{I}_2), \quad m \in [1, \cdots, M], \tag{13}$$

where $\mathbf{w}_m^{(l)} = [w_{mR}^{(l)}, w_{mI}^{(l)}]^T$ is a two-element vector consisting of the real and imaginary parts of the m-th scattering coefficient. It is emphasized that, because α_m, to be determined later, varies with each pixel, the overall distribution of the reflection coefficients does not assume a specific distribution across the scene.

It is important to note that the parameters $\boldsymbol{\alpha} = \{\alpha_m\}_{m=1,M}$ assume identical values for their real and imaginary components and across the L groups. The m-th complex scattering coefficients tend to be zero with probability 1 across L groups when α_m is set to zero.[14] By setting equal α_m for the real and imaginary parts, instead of treating them separately as in,[15,16,24] the CMT-BCS algorithm not only enhances the sparsity of the problem, but exploits both real and imaginary components for better estimation of the shared parameters α_m. The benefits of this approach will be clearly demonstrated in the simulation section.

To promote sparsity over the scattering coefficients $\mathbf{w}^{(l)}$, a Gamma prior is placed on α_m^{-1}, i.e.,[12]

$$\alpha_m^{-1} \sim \text{Gamma}(\alpha_m^{-1}|a, b), \tag{14}$$

where

$$\text{Gamma}(x^{-1}|a, b) = \Gamma(a)^{-1} b^a x^{-(a-1)} e^{-\frac{b}{x}}, \tag{15}$$

and $\Gamma(\cdot)$ denotes the Gamma function.

It has been demonstrated in[12] that an appropriate choice of the parameters a and b encourage a sparse representation for the coefficients in the $\mathbf{w}^{(l)}$. Typically, when a and b are small constants, α_m^{-1} that draws from $\text{Gamma}(\cdot|a, b)$ has a large spike concentrated at zero and a heavy right tail.

Without loss of generality, a Gaussian prior is placed on the additive measurement noise, i.e.,

$$\boldsymbol{\varepsilon}_m^{(l)} \sim \mathcal{N}(\boldsymbol{\varepsilon}_m^{(l)}|\mathbf{0}, \beta_0 \mathbf{I}_2), \tag{16}$$

where $\boldsymbol{\varepsilon}_m^{(l)}$ is a two-element vector consisting of the real and imaginary parts of the complex noise, and β_0 is the noise variance. Similar to $\boldsymbol{\alpha}$, we place β_0^{-1} on the Gamma prior with parameters c and d, where $c = d = 0$ are used as a default choice.[12]

Now, we consider the posterior probability density function of

$$\mathbf{w}^{(l)} = [w_{1R}^{(l)}, \cdots, w_{MR}^{(l)}, w_{1I}^{(l)}, \cdots, w_{MI}^{(l)}]^T. \tag{17}$$

By assuming that the parameters $\boldsymbol{\alpha}$ and β_0 are known (their derivations will be discussed in the later part of this section), the posterior distribution of $\mathbf{w}^{(l)}$ is evaluated analytically based on Bayes' rule as,

$$\Pr(\mathbf{w}^{(l)}|\mathbf{y}^{(l)}, \mathbf{\Phi}^{(l)}, \boldsymbol{\alpha}, \beta_0) = \mathcal{N}(\mathbf{w}^{(l)}|\boldsymbol{\mu}^{(l)}, \mathbf{\Sigma}^{(l)}), \tag{18}$$

where

$$\boldsymbol{\mu}^{(l)} = \beta_0^{-1}\boldsymbol{\Sigma}^{(l)}(\boldsymbol{\Psi}^{(l)})^T\tilde{\mathbf{y}}^{(l)}, \tag{19}$$

$$\boldsymbol{\Sigma}^{(l)} = \left(\beta_0^{-1}(\boldsymbol{\Psi}^{(l)})^T\boldsymbol{\Psi}^{(l)} + \mathbf{A}^{-1}\right)^{-1}, \tag{20}$$

$$\boldsymbol{\Psi}^{(l)} = \begin{bmatrix} \mathrm{Re}(\boldsymbol{\Phi}^{(l)}) & -\mathrm{Im}(\boldsymbol{\Phi}^{(l)}) \\ \mathrm{Im}(\boldsymbol{\Phi}^{(l)}) & \mathrm{Re}(\boldsymbol{\Phi}^{(l)}) \end{bmatrix}, \tag{21}$$

$$\mathbf{A} = \mathrm{diag}(\alpha_1, \cdots, \alpha_M, \alpha_{M+1}, \cdots, \alpha_{2M}), \tag{22}$$

$$\alpha_i = \alpha_{i+M}, \quad i \in [1, \cdots, M], \tag{23}$$

and $\tilde{\mathbf{y}}^{(l)} = [\mathrm{Re}(\mathbf{y}^{(l)}), \mathrm{Im}(\mathbf{y}^{(l)})]^T$. Note that, contrary to the approach taken in[15,16,24] where the real and imaginary components assume different prior parameters, we force the restriction condition (23) on the shared parameters so that the sparsity is reduced by a factor of two.

With known $\boldsymbol{\alpha}$ and β_0, the mean and covariance of each scattering coefficient was derived in (19) and (20). The associated learning problem, in the context of the RVM, thus becomes a search for the parameters $\boldsymbol{\alpha}$ and β_0. A fast learning algorithm of $\boldsymbol{\alpha}$ was proposed and the updated expression of $\boldsymbol{\alpha}$ is expressed as in,[19]

$$\alpha_m^{(\mathrm{new})} = \sqrt{\frac{\sum_{l=1}^{L}\left(\mathbf{w}_m^{(l)}\right)^T\mathbf{w}_m^{(l)} + \left(\mathbf{w}_{m+M}^{(l)}\right)^T\mathbf{w}_{m+M}^{(l)}}{\sum_{l=1}^{L}\mathrm{Tr}\left[\mathbf{C}_l^{-1}\left(\left(\boldsymbol{\Psi}_m^{(l)}\right)^T\boldsymbol{\Psi}_m^{(l)} + \left(\boldsymbol{\Psi}_{m+M}^{(l)}\right)^T\boldsymbol{\Psi}_{m+M}^{(l)}\right)\right]}}, \tag{24}$$

in which $\mathbf{C}_l = \beta_0\mathbf{I} + \boldsymbol{\Psi}^{(l)}\mathbf{A}(\boldsymbol{\Psi}^{(l)})^T$. $\boldsymbol{\Psi}_m^{(l)}$ and $\boldsymbol{\Psi}_{m+M}^{(l)}$, which are respectively the m-th and $(m+M)$-th columns in the $\boldsymbol{\Psi}^{(l)}$, function as the corresponding real and imaginary atoms for the m-th scattering coefficient $\mathbf{w}_m^{(l)} = [\mathbf{w}_{mR}^{(l)}, \mathbf{w}_{mI}^{(l)}]$. Also, the noise precision β_0 is updated by[19,25,26]

$$\beta_0^{(\mathrm{new})} = \frac{\sum_{l=1}^{L}\mathrm{Tr}[\boldsymbol{\Sigma}^{(l)}\boldsymbol{\Psi}^{(l)}(\boldsymbol{\Psi}^{(l)})^T] + \|\tilde{\mathbf{y}}^{(l)} - \boldsymbol{\Psi}^{(l)}\boldsymbol{\mu}^{(l)}\|_2^2}{2ML}. \tag{25}$$

Note that $\boldsymbol{\alpha}^{(\mathrm{new})}$ and $\beta_0^{(\mathrm{new})}$ are functions of $\{\mathbf{w}^{(l)}\}_{l=1}^L$, $\{\boldsymbol{\mu}^{(l)}\}_{l=1}^L$ and $\{\boldsymbol{\Sigma}^{(l)}\}_{l=1}^L$, while $\{\mathbf{w}^{(l)}\}_{l=1}^L$, $\{\boldsymbol{\mu}^{(l)}\}_{l=1}^L$ and $\{\boldsymbol{\Sigma}^{(l)}\}_{l=1}^L$ are functions of $\boldsymbol{\alpha}$ and β_0. This suggests an iterative algorithm, which iterates (18), (19), (20) and (24), (25), until a convergence criterion is satisfied.

4. SIMULATION RESULTS

In the simulation, DVB-T signals with a carrier frequency of 850 MHz and a bandwidth of 7.8 MHz which corresponds to around 20 m range resolution is used in the simulations. The simulation scene is illustrated in Fig. 2(a), where the azimuth angle width of the receiver corresponding to each illuminator is 5°, and thus the conventional azimuth resolutions are around 5 m. The three illuminators are located 10 km away from the scene center with their respective aspect angles of −45°, 0°, and 45°. These illuminators emit their individual DVB-T waveforms to the scene with different frequencies. The complex scattering coefficients assume the same value over the 5° angle for each illuminator, but vary with different illuminators due to the distinct aspect angles. 64 synthetic aperture positions are acquired by uniformly dividing the synthetic aperture width.

The sparse scene being considered, as depicted in Fig. 2(b), consists of 32×32 pixels. With the consideration of the sparsity measure[27] that most signals can be recovered by the l_1 norm minimization, we choose the total number of sparse targets to be $Q = 19$. The inter-pixel spacings are 1m in both range and azimuth.

According to the conventional SAR imaging principle, high resolution is achieved by exploiting a wide coherent synthetic aperture. However, we cannot coherently accumulate the data acquired in all bistatic pairs due to the angle-dependent scattering coefficients. As such, without considering the group sparsity, we form individual images separately for each bistatic pairs based on CMT-BCS with $L = 1$. The result of incoherently fusing these

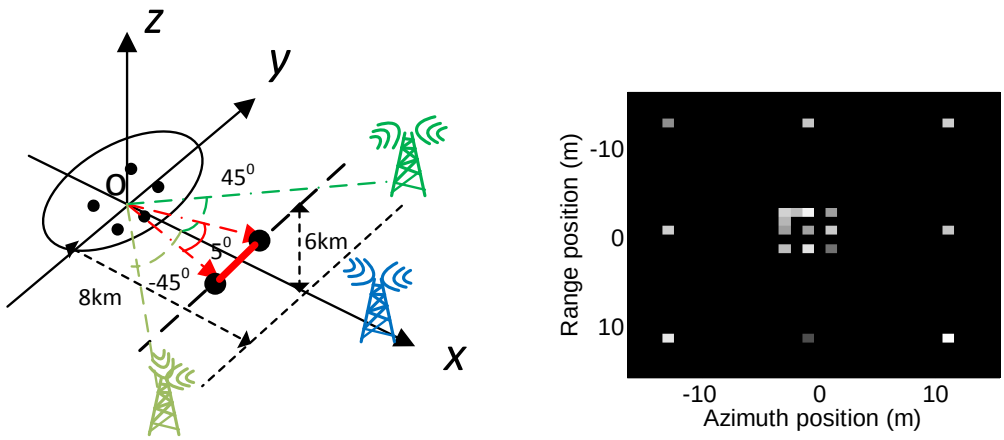

(a) (b)

Figure 2. (a) Geometry of multi-static passive SAR system. (b) Normalized magnitude of the scattering coefficients of the original scene.

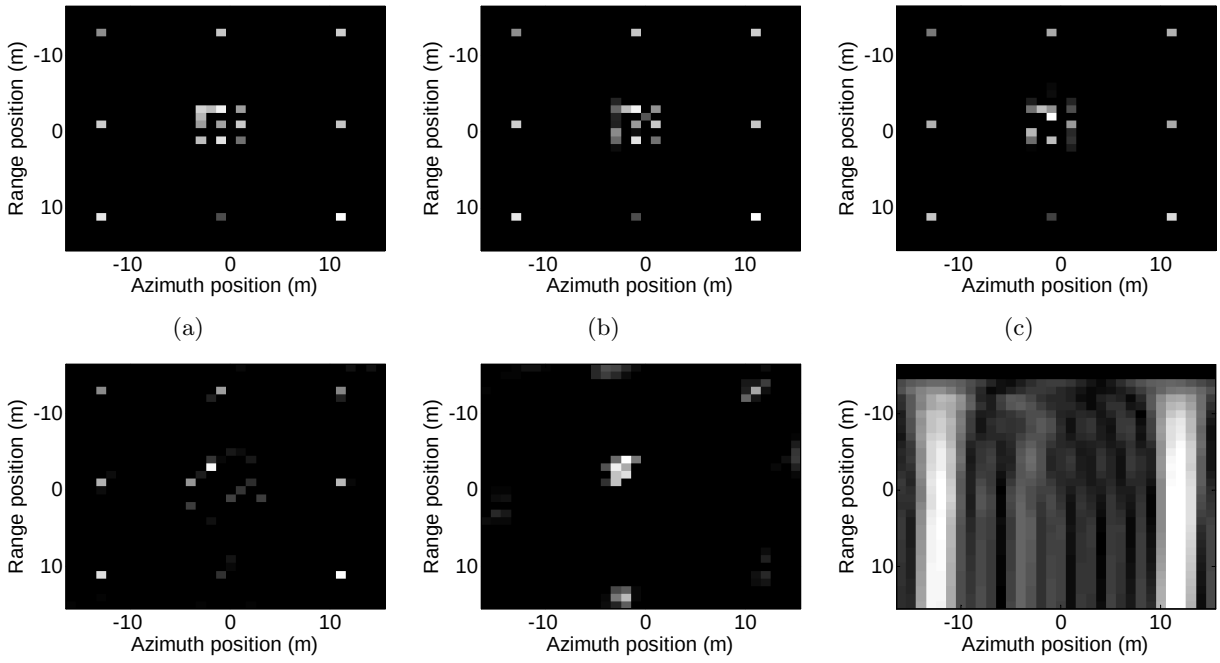

(a) (b) (c)

(d) (e) (f)

Figure 3. Reconstruction results in the multi-static passive SAR system. (a) Reconstructed result based on CMT-BCS. (b) Fused image based on three sub-images. (c) Reconstructed result based on mt-CS. (d) Reconstructed result based on gLasso. (e) Reconstructed result based on BOMP. (f) Reconstructed result based on FBP.

three sub-images is shown in Fig. 3(b). It is clear from the fused image that the targets within one conventional range cell (20 m) are resolved, but the resulting image shows much more spurious targets.

Now, we compare the performance of the CMT-BCS to selected existing techniques, including the mt-CS, gLasso, BOMP, and filtered backprojection (FBP).[5] As shown in Figs. 3(f) and 3(e), the FBP and BOMP algorithms yield very poor image qualities. Among them, the FBP imaging algorithm has no super-solution capability and all the targets in the same range resolution cell cannot be resolved. The BOMP algorithm is suited to recover sparse signals when the measurement matrix has a low coherence. In the underlying scenario, however, the coherence between the columns of the measurement matrix $\mathbf{\Phi}$ is as high as 0.97. The result of the gLasso algorithm is shown in Fig. 3(d). The gLasso is able to recover moderately separated targets but fails to resolve closely spaced targets. The mt-CS algorithm, as one of sparse Bayesian learning based on RVM, has a better performance than the other three algorithms, as it is less sensitive to the high coherence of the dictionary $\mathbf{\Phi}$. However, because it treats the real and imaginary components of the reflection coefficients independently, the mt-CS result depicted in Fig. 3(c) yields a number of undesired spurious targets. In conclusion, the CMT-BCS algorithm achieves improved capability of reconstructing super-resolution imaging in a multi-static scenario characterized by a complex group sparsity model.

5. CONCLUSION

Passive synthetic aperture radar (SAR) systems suffer from low range resolution due to their low carrier frequency and narrow signal bandwidth. A novel super-resolution sparse Bayesian learning technique, namely, complex multi-task Bayesian compressive sensing (CMT-BCS) algorithm, was exploited to acquire super-resolution images in a multi-static passive radar system, where the scattering coefficients are assumed to have a common sparse support for all bistatic pairs but the values vary with each bistatic pair.

ACKNOWLEDGMENTS

The work of Q. Wu, Y. D. Zhang, and M. G. Amin was supported in part by a subcontract with Defense Engineering Corporation for research sponsored by the Air Force Research Laboratory under Contract FA8650-12-D-1376 and by a subcontract with Dynetics, Inc. for research sponsored by the Air Force Research Laboratory under Contract FA8650-08-D-1303.

REFERENCES

1. I. G. Cumming and F. H. Wong, *Digital Processing of Synthetic Aperture Radar Data: Algorithms and Implementation*. Artech House, 2005.
2. H. Griffiths and N. Long, "Television-based bistatic radar," *Proc. IEE-Radar Sonar Navig.*, vol. 133, no. 7, pp. 649–657, 1986.
3. H. D. Griffths and C. J. Baker, "Passive coherent location radar systems. part 1: Performance prediction," *Proc. IEE-Radar Sonar Navig.*, vol. 152, no. 3, pp. 153–159, 2005.
4. Y. D. Zhang and B. Himed, "Moving target parameter estimation and SFN ghost rejection in multistatic passive radar," in *Proc. IEEE Radar Conf.*, Ottawa, Canada, April 2013.
5. C. E. Yarmanb and B. Yazici, "Passive synthetic aperture radar imaging of ground moving targets," *in Proc. SPIE*, vol. 8394, 2012.
6. X. Mao, Y. D. Zhang, and M. G. Amin, "Two-stage multi-static passive sar imaging with reduced complexity," in *Proc. IEEE Radar Conf.*, Cincinnati, OH, May 2014.
7. M. Yuan and Y. Lin, "Model selection and estimation in regression with grouped variables," *Journal of the Royal Statistical Society Series B*, vol. 68, no. 1, pp. 49–67, 2006.
8. L. Jacob, G. Obozinski, and J. Vert, "Group Lasso with overlap and graph Lasso," *Proc. Int. Conf. on Machine Learning*, vol. 49, no. 10, pp. 3993–4006, 2009.
9. J. Huang and T. Zhang, "The benefit of group sparsity," *Ann. Statist.*, vol. 38, no. 4, pp. 1978–2004, 2010.
10. V. Temlyakova and P. Zheltova, "On performance of greedy algorithms," *Journal of Approximation Theory*, 2010.
11. S. Ji, Y. Xue, and L. Carin, "Bayesian compressive sensing," *IEEE Trans. Signal Proc.*, vol. 56, no. 6, pp. 2346–2356, 2008.
12. M. E. Tipping, "Sparse Bayesianshrinkage and selection learning and the relevance vector machine," *Journal of Machine Learning Research*, vol. 1, no. 9, pp. 211–244, 2001.

13. Z. Zhang and B. D. Rao, "Sparse signal recovery with temporally correlated source vector using sparse bayesian learning," *IEEE Jounal of Selecteed Topics in Signal Processing*, vol. 5, no. 5, pp. 1–15, 2011.
14. S. Ji, D. Dunson, and L. Carin, "Multi-task compressive sampling," *IEEE Trans. Signal Proc.*, vol. 57, no. 1, pp. 92–106, 2009.
15. G. Oliveri, P. Rocca, and A. Massa, "A Bayesian compressive sampling-based inversion for imaging sparse scatterers," *IEEE Trans. Geosci. Remote Sens.*, vol. 49, no. 10, pp. 3993–4006, 2013.
16. M. Carlin, P. Rocca, G. Oliveri, F. Viani, and A. Massa, "Directions-of-arrival estimation through bayesian compressive sensing strategies," *IEEE Trans. Antennas and Propagation.*, vol. 61, no. 7, pp. 3828–3838, 2013.
17. Y. D. Zhang and B. Himed, "Space-time adaptive processing in bistatic passive radar exploiting complex Bayesian learning," in *Proc. IEEE Radar Conf.*, Cincinnati, OH, May 2014.
18. M. G. Amin, Y. D. Zhang, and B. Jokanovic, "Time-frequency signature reconstruction from random observations using multiple measurement vectors," in *Proc. IEEE Int. Conf. Acoustics, Speech, and Signal Processing*, Florence, Italy, May 2014.
19. Q. Wu, Y. D. Zhang, M. G. Amin, and B. Himed, "Complex multitask Bayesian compressive sensing," in *Proc. IEEE Int. Conf. Acoustics, Speech, and Signal Processing*, Florence, Italy, May 2014.
20. C. Nolan and M. Cheney, "Synthetic aperture inversion for arbitrary flight paths and non-flat topography," *IEEE Trans. Image Proc.*, vol. 12, no. 4, pp. 1035–1043, 2003.
21. C. E. Yarmanb, L. Wang, and B. Yazici, "Doppler synthetic aperture hitchhiker imaging," *Inverse Probl.*, vol. 26, no. 6, pp. 1–26, 2010.
22. L. Wang, C. E. Yarmanb, and B. Yazici, "Doppler-hitchhiker: A novel passive synthetic aperture radar using ultra-narrowband sources of opportunity," *IEEE Trans. Geosci. Remote Sens.*, vol. 49, no. 10, pp. 3521–3537, 2011.
23. R. G. Baraniuk, "Compressive sampling," *IEEE Signal Process. Mag.*, vol. 24, no. 4, pp. 118–124, 2007.
24. Z. Zhang, "Complex-valued problem in the BSBL algorithm," *https://sites.google.com/site/researchbyzhang/bsbl.* Accessed on Feb. 25, 2014.
25. Z. Zhang and B. D. Rao, "Extension of SBL algorithm for the recovery of block sparse signals with inter-block correlation," *IEEE Trans. Signal Proc.*, vol. 92, no. 7, pp. 1580–1590, 2012.
26. P. Stoica and P. Babu, "Spice and likes: Two hyperparameter-free methods for sparse-parameter estimation," *Signal Processing*, vol. 92, no. 7, pp. 1580–1590, 2012.
27. D. L. Donoho and J. Tanner, "Counting faces of randomly projected polytopes when the projection radically lowers dimensions," Technical Report, Department of Statistics, Stanford University, 2006.